IN-02
14438
P19

NASA Technical Memorandum 104377

Euler Flow Predictions for an Oscillating Cascade Using A High Resolution Wave-Split Scheme

Dennis L. Huff
Lewis Research Center
Cleveland, Ohio

Timothy W. Swafford
Mississippi State University
Mississippi State, Mississippi

T.S.R. Reddy
The University of Toledo
Toledo, Ohio

Prepared for the
36th International Gas Turbine and Aeroengine Congress and Exposition
sponsored by the American Society of Mechanical Engineers
Orlando, Florida, June 3-6, 1991

NASA

(NASA-TM-104377) EULER FLOW PREDICTIONS FOR AN OSCILLATING CASCADE USING A HIGH RESOLUTION WAVE-SPLIT SCHEME (NASA) 19 P
CSCL 01A
N91-24107
Unclas
G3/02 0014438

Euler Flow Predictions for an Oscillating Cascade Using a High Resolution Wave-Split Scheme

Dennis L. Huff
National Aeronautics and Space Administration
Lewis Research Center
Cleveland, OH

Timothy W. Swafford*
Mississippi State University
Mississippi State, MS

T.S.R. Reddy†
The University of Toledo
Toledo, OH

ABSTRACT

A compressible flow code that can predict the nonlinear unsteady aerodynamics associated with transonic flows over oscillating cascades is developed and validated. The code solves the two-dimensional, unsteady Euler equations using a time-marching, flux-difference splitting scheme. The unsteady pressures and forces can be determined for arbitrary input motions, although this paper will only address harmonic pitching and plunging motions. The code solves the flow equations on a H-grid which is allowed to deform with the airfoil motion. Predictions are presented for both flat plate cascades and loaded airfoil cascades. Results are compared to flat plate theory and experimental data. Predictions are also presented for several oscillating cascades with strong normal shocks where the pitching amplitudes, cascade geometry and interblade phase angles are varied to investigate nonlinear behavior.

NOMENCLATURE

$\overline{A}$	Roe matrix
c	chordlength
C_l	lift coefficient, $\frac{l}{c\rho V_1^2}$
C_m	moment coefficient, $\frac{m}{c^2\rho V_1^2}$
CP	pressure coefficient, $\frac{p-p_1}{\frac{1}{2}\rho_1 V_1^2}$
ΔCP	pressure difference coefficient, $\frac{p_- - p_+}{\rho_1 V_1^2 \lvert\alpha_1\rvert}$
F,G,H	flux vectors
h_1	amplitude of oscillation for plunging motions based on chordlength
i	incidence angle (Figure 1)

*Summer Faculty Fellow at NASA Lewis Research Center.
†NASA Resident Research Associate at Lewis Research Center.

Im{ }	imaginary part of { }
k	reduced frequency based on semi-chord
l	lift
m	moment
M	Mach number
Ma{ }	magnitude of { }
N	number of airfoils in cascade
p	static pressure
p_0	total pressure
Q	dependent variable vector
Re{ }	real part of { }
s	cascade spacing (Figure 1)
t,τ	time
t/c	airfoil thickness-to-chord ratio
V	total velocity
x,y	spatial coordinates
α_1	amplitude of oscillation for pitching motions
γ	stagger angle (Figure 1)
ξ, η, ζ	curvilinear coordinate directions
ρ	fluid density
σ	interblade phase angle
Subscripts	
1,2	conditions at inlet/exit
+,-	upper/lower surfaces on airfoil
L,R	left/right of an interface
r	condition at acoustic resonance
Superscripts	
n	time index

INTRODUCTION

The accurate prediction of flutter and fatigue in turbomachinery blades is always essential for designers in the propulsion industry. Designing against flutter and fatigue failures becomes a challenge as structural designs become less conservative. Examples include recent advanced turboprops and ducted propellers. Flutter becomes more of a problem with increased sweep of the blades. Also, since these designs operate at an angle of attack with respect to the flight direction, periodic forces on the blades must be modeled. Recent computations from an unsteady, three-dimensional Euler code indicate that the unsteady power per blade may vary by as much as eighty percent of the mean power for an advanced turboprop (SR-7) operating with a 4.6 degree inflow angle (ref.1). The installation of struts and wings near the propeller also introduces unsteady forces that may cause fatigue failures. Since these flows are typically transonic and highly three-dimensional, the accurate prediction of the steady and unsteady flowfields can be difficult and time consuming.

A two-dimensional oscillating cascade is often used to model the unsteady forces on an airfoil due to flutter or forced response. In the case of forced response, a simulation of the once-per-revolution variation of blade incidence angle can be modeled for a propeller at angle of attack. For flutter, harmonic analysis is often used to determine when the flow is doing positive work on the blades, which can cause an instability. Special cases from a two-dimensional analysis have exact solutions available that can be used to test a new idea or algorithm. Using flat plates instead of airfoils allows for exact comparisons with small-perturbation theory. This is a necessary step for flutter and forced response analysis due to the limited amount of experimental data available for transonic flows at realistic forcing frequencies.

There are a number of numerical and analytical methods available for addressing the two-dimensional, oscillating cascade problem. Time linearized analysis has been used the most in aeroelasticity for current designs since it does a reasonably good job near design conditions and is inexpensive to run. Another advantage to time-linearized approaches is exact specification of the far-field boundary conditions. Codes in this category include the work by Smith (ref.2), which is valid for flat plates in subsonic flow, and Verdon (ref.3), which accounts for blade loading effects in transonic flow. While the latter solves the linearized full-potential equations, work has also been reported by Hall and Crawley (ref.4) that solves the linearized Euler equations. Time-marching schemes are also available that solve the full-potential (ref.5), Euler (refs. 6,7,8,9), and Navier-Stokes (ref.7) equations. Two fundamental problems exist for the time-marching codes: 1.) Specification of correct unsteady inflow/outflow boundary conditions and 2.) Reduction of computational time. In spite of these problems, reasonable solutions have been obtained when compared to linear theory and experimental data. The time-marching codes, although expensive to run, gives researchers a way to investigate nonlinear solutions. The prediction of the nonlinear flowfield is expected to be important in transonic flow with moderate shock motion. Since it is not possible to assess these effects with a linear code, the time-marching codes that solve the nonlinear flowfield are a necessary research tool. The reader is referred to a recent review by Bendiksen (ref.10), which identifies applications where nonlinear phenomena may be important. Reference 10 also identifies more codes that have been developed for modeling oscillating cascade flows.

The objective of this work is to develop and validate a compressible flow code that can predict the nonlinear unsteady aerodynamics associated with transonic flows over oscillating cascades. The present code solves the unsteady Euler equations using the time-marching, flux-difference splitting scheme of Whitfield, et al. (ref.11) using blocked grids. The grid motion was added to the code for modeling the oscillating cascade problem. While other Euler codes (refs. 6,7,8,9) exist for predicting these flows, this is the first application of a flux-splitting algorithm. The code solves the flow equations using one or more H-grid, which are allowed to deform with the airfoil motion similar to the method developed in reference 7. The unsteady pressures and blade forces can be determined for arbitrary input motions, although this paper will only address harmonic pitching and plunging motions. Predictions are presented in this work for both flat plate cascades and loaded airfoil cascades. Results are compared to flat plate theory and experimental data. Predictions are also presented for several oscillating cascades with strong normal shocks where the pitching amplitudes, cascade geometry and interblade phase angles are varied to investigate nonlinear behavior.

GOVERNING EQUATIONS AND NUMERICAL ALGORITHM

Only inviscid Euler solutions are sought in the present analysis, although viscous effects must ultimately be included to properly account for all pertinent flowfield features. This expedites the solution process and makes possible a one-to-one comparison between results obtained herein and those generated by previous methods, both Euler and potential. Therefore, the unsteady three-dimensional Euler equations written in conservative differential form are used and are transformed from a Cartesian to a time-dependent curvilinear reference frame. This transformation process and the ensuing numerical method are presented in detail in references 11-15. Hence the following discussion merely highlights the development of the methodology and the reader is encouraged to consult the above references for more detail.

The transformed equations can be written in vector form as

$$\frac{\partial Q}{\partial \tau} + \frac{\partial F}{\partial \xi} + \frac{\partial G}{\partial \eta} + \frac{\partial H}{\partial \zeta} = 0 \qquad (1)$$

where the dependent variable vector Q and fluxes F, G, and H are presented in references 11-14. The present applications will only consider two-dimensional solutions to these equations, but three-dimensional formulation will be presented here for generality. The approach taken in the present effort is based on the integration of

these equations over a discrete set of contiguous cells (volumes) in computational space and is generally referred to as a finite volume method. This discretization results in the following expression where cell centers are denoted as i,j,k:

$$\frac{\partial Q}{\partial \tau} + \frac{\delta_i F}{\Delta \xi} + \frac{\delta_j G}{\Delta \eta} + \frac{\delta_k H}{\Delta \zeta} = 0 \tag{2}$$

With $\Delta\xi = \Delta\eta = \Delta\zeta = 1$ (by definition), this becomes

$$\frac{\partial Q}{\partial \tau} = -(\delta_i F + \delta_j G + \delta_k H) \tag{3}$$

where

$$\delta_*(.) = (.)_{*_{1/2}} - (.)_{*_{-1/2}}. \tag{4}$$

A consequence of the finite volume formulation is that components of the dependent vector Q within a particular cell represent average values over that cell. However, it is evident from the above representation of flux differences that a method is needed to allow these fluxes to be accurately represented at cell faces. As discussed in reference 11, the method used in the present effort is based on the one-dimensional approximate Riemann solver of Roe (ref.16) at cell interfaces for each coordinate direction. The method uses as a basis the following approximate equation which represents a quasilinear form of a locally one-dimensional conservation law:

$$\frac{\partial q}{\partial t} + \bar{A}(q_L, q_R)\frac{\partial q}{\partial x} = 0 \tag{5}$$

where q is the untransformed dependant variable vector, and $\bar{A}(q_L, q_R)$ is a constant matrix representative of local cell interface conditions and is constructed using so-called "Roe averaged" variables. The determination of the eigensystem of $\bar{A}$ and knowing that the change in dependent variables across an interface is proportional to the right eigenvectors allows first order flux formulae to be constructed. This approach of extracting flowfield information from characteristically dictated directions is commonly referred to as flux difference splitting (FDS) and is applicable to multidimensional space, so long as the assumption is made that all wave propagation occurs normal to a particular cell interface. To provide higher order spatial accuracy, a corrective flux is appended to the first order flux discussed above. In addition, in order to control dispersive errors commonly encountered with higher order schemes, so-called "limiters" are used to limit components of the interface flux resulting in total variation diminishing (TVD) schemes. All solutions presented herein were obtained using the basic algorithm developed in reference 11, which is third-order accurate spatially and second-order accurate in time.

GRID

The flow equations are solved within one or more passage centered H-grids, where the number of grids depends on the interblade phase angle (see equation 6 below). Within a typical grid block, the lower computational boundary contains the upper surface of one blade in the cascade, while the upper computational boundary contains the lower surface corresponding to the adjacent blade. Periodic boundaries in the blade-to-blade direction extend upstream and downstream from the blade surfaces. The inlet boundary corresponds to the left computational boundary and the outflow corresponds to the right boundary (Figure 1a). The grid was generated using a two-dimensional version of the IGB code developed by Beach (ref.17) for turbomachinery. This grid generator gives the user good flexibility and control over the features in the H-grid. This includes modeling rounded leading and trailing edges (which is important for predicting shocks in transonic flows), grid spacing near the airfoil, and global or local smoothing. The grid generator runs interactively on an IRIS-4D workstation and saves a journal file for grid reproduction. Once a grid is generated for a single blade passage, it is stacked to form a cascade for multiple blades.

For unsteady flows, where the blades undergo harmonic oscillations, the number of airfoils (or grid blocks) needed for modeling an infinite cascade is a function of the inter-blade phase angle (σ) and is obtained using the following relationships:

$$N = \frac{2\pi}{\sigma} \quad , \quad where \quad 0 < \sigma \leq 2\pi \tag{6}$$

For example, a $\sigma = 2\pi$ case (in-phase motion) requires one block, $\sigma = \pi$ two blocks, etc. One can see how the number of blocks required to model all interblade phase angles can become quite large. Fortunately, the range of interblade phase angles of interest for flutter analysis is limited by the number of blades on the rotor. For a propfan, this is usually between 8 and 12 blades. Several researchers have investigated methods for reducing the computational domain to a single or several passages. One method (ref.5) uses a time shearing approach developed by Giles (ref.18) to specify the upper and lower periodic boundaries for a single passage. Another technique (ref.19) uses an influence coefficient approach and uses information from one airfoil oscillating in the cascade to determine the unsteady pressures as though all airfoils were oscillating. The results from both of these methods look promising, but they do introduce approximations to the solutions. For now, all airfoils will be oscillated and exact periodic boundary conditions will be imposed to eliminate a possible source for error.

The code can simulate both pitching and plunging motions, either individually or in combination. The computational grid is deformed such that the airfoils follow the prescribed motion and the grid near the center of the passage remains fixed. This is done using weighting functions and is similar to the method presented in reference 7 for C-grids, except the current method is for H-grids. For a given blade passage, the upper and lower boundaries containing the airfoil surfaces move according to an input function (which may come from the displacements calculated from a structural model). For a specified interblade phase angle, the grid deforms for a single blade passage for one cycle of oscillation and saves the grids for N blades corresponding to σ. Each grid is stored on the Solid State Storage Device (SSD) on the CRAY computer. Once the initial grid has been defined for all blade passages, the code time-marches the grid and the flow solution for harmonic oscillations, preserving the specified interblade phase angle.

BOUNDARY CONDITIONS

Because the computational grids used in the present study employ multiple blocks, a discussion pertaining to how flowfield conditions are imposed along the boundaries of the computational domain is needed.

Single Blade Passage ($\sigma = 0$)

Figure 1a represents a single grid block used for zero interblade phase angle cases. The airfoil upper and lower surfaces are located along lines B-C and F-G, respectively, where solid wall boundary conditions are employed. (Phantom cells were used to enforce all boundary conditions in the present studies). Lines A-E and D-H represent subsonic inflow and outflow boundaries, respectively, where conditions were set using characteristic variable boundary conditions, as derived in references 20 and 21. The procedure was to fix the incoming flow incidence angle and adjust the back pressure (uniform across D-H) until the average Mach number along the inflow boundary (A-E) matched some predetermined value. Periodicity was imposed between lines A-B and E-F, and lines C-D and G-H, respectively.

Multiple Blade Passages ($\sigma \neq 0$)

For non-zero interblade phase angles (ie. multiple blocks), additional grid blocks (passages) are stacked, as shown in Figure 1b for $\sigma = 180$ degrees. For this case, periodicity is enforced between lines A-B and I-J, and lines C-D and K-L, respectively. Also lines A-I and D-L become inflow and outflow boundaries, respectively. Continuity of flowfield variables is imposed between adjacent blocks (E-F and G-H) by simple injection (see Figure 1b with regard to the use of interior and phantom cells of adjacent blocks). A similar procedure is followed for other interblade phase angles which require additional blade passages (equation 6).

RESULTS AND DISCUSSION

Code validation is done by comparing solutions for flat plate cascades with predictions from small-perturbation methods. Also, comparisons with experimental data are included for a loaded biconvex airfoil cascade. Solutions are then presented that predict the onset of nonlinear behavior based on variation of the oscillation amplitude.

Code Validation

All of the Euler solutions were executed on a 121 x 41 (streamwise x pitchwise) grid, typical to the grid shown in Figure 1a. Coarser grids were tried and gave satisfactory results, however a finer grid is used here to eliminate grid resolution as a source for error. The inlet boundary is located 1.5 chordlengths upstream from the stagger line and uses 35 nodes in the streamwise direction. There are 60 points along each surface of the airfoil and clustered about the leading and trailing edges. The grid extends downstream 1.5 chordlengths from the trailing edge. The solutions were executed on a CRAY-YMP computer and require about 5×10^{-5} CPU seconds per grid point per iteration. A constant time step is used, which means the CFL number varies as a function of the grid spacing. In regions where the grid is clustered, the CFL number increases significantly. For the grids used in the following results, a maximum CFL number of 60 is used, which occurs near the leading and trailing edges. The CFL numbers quickly drop to values ranging from 2 to 6 in regions away from the leading and trailing edges. For several special cases, the maximum CFL number is lowered to 10 in order to assess dispersion errors, which corresponds to most of the grid cells having a CFL number less than one.

Flat Plate Cascades

i) Pitching Motions

For a cascade of flat plates in subsonic flow, the small-perturbation theory of Smith (ref.2) can be used for exact comparisons. The geometry from the experiment in reference 19 is used, except flat plates are used instead of the biconvex airfoils. A test case has been selected from the experiment as follows: $M_1 = 0.80$, $k = 0.32$, $\gamma = 45$ degrees, s/c = 1.538, i = 0 degrees, $\alpha_1 = 1.2$ degrees.

The lift coefficient versus time is shown in Figure 2 for $\sigma = -90$ degrees and is typical of other results from the Euler code. The results from each cycle of oscillation are read into a fast Fourier transform (FFT) subroutine to obtain the harmonic content and determine the solution periodicity. The airfoils are pitched about the mid-chord for three cycles of oscillation, which was found to be long enough for the solutions to become periodic in time. Euler solutions were found for $\sigma = -90$, 0, and 90 degrees. The first harmonic pressure difference coefficient distribution are presented in Figures 3 and 4 for $\sigma = -90$ and 90 degrees, respectively, which are typical of the best and worse agreement with theory. The results from the theory of Smith are also plotted for comparison. The real and imaginary parts of the first harmonic moment coefficient are given in Table I.

An investigation was done for $\sigma = 90$ by lowering the pitching amplitude to 0.1 degrees to make sure that the small-perturbation assumption was not violated. This was found to give only slightly better predictions than the higher amplitude (see Table I). One possible reason for discrepancies as a function of σ is the specification of the far-field boundary conditions, as described below.

Buffum, et al. (ref.19) has calculated the sub-resonant and super-resonant regions for this cascade based on a method by Smith (ref.2). The interblade phase angles corresponding to resonant conditions are calculated as follows based on the flow upstream of the cascade:

$$\sigma_r = \frac{2kM_1 s}{c(1-M_1^2)}\left[M_1 \sin(i+\gamma) \pm \sqrt{1 - M_1^2 \cos^2(i+\gamma)}\right] \qquad (7)$$

The resonant interblade phase angles for the present cascade are $\sigma_r = -31.7$ degrees and $\sigma_r = 178.4$ degrees. The interblade phase angles that lie between these values are super-resonant, which means that the pressure waves will propagate upstream and downstream to infinity without decay. Interblade phase angles above and below the higher and lower resonant values are sub-resonant, where pressure waves decay with distance from the cascade. For the current test case; when $\sigma = -90$ degrees, the cascade is sub-resonant. This is a condition where the numerical results are expected to be relatively insensitive to reflections from the inflow and outflow

boundaries, assuming the boundaries are sufficiently removed from the cascade. On the other hand, when σ = 90 degrees, the cascade is super-resonant, and the results become sensitive to the boundary conditions used for both the inflow and outflow.

ii) Plunging Motions

Results are presented for a flat plate cascade undergoing plunging motions and are compared with the theory of Smith (ref.2) and Verdon's LINFLO code (ref.22). The test cases were selected from Verdon and Casper (ref.22) for comparisons of the unsteady pressure distributions: M_1 = 0.70, k = 0.50, γ = 45 degrees, s/c = 1., i = 0, (and h_1 = 0.01 for the Euler solutions). Figure 5 shows comparisons for σ = 0 , which corresponds to a super-resonant condition and Figure 6 shows comparisons for σ = 180 degrees, which is sub-resonant. As for the pitching motion cases, the agreement between the Euler predictions and the small-perturbation methods is not as good for super-resonant conditions. However, the overall agreement is good between all three prediction methods.

Biconvex Airfoil Cascades

Solutions are now presented for a cascade of biconvex airfoils, where experimental data (ref.19) are available for comparisons at various Mach numbers and reduced frequencies. The experimental cascade consists of four biconvex airfoils with a thickness-to-chord ratio (t/c) of 0.076, c/s = 0.65, γ = 45 degrees, and i = 2 degrees. In the Euler solutions, the leading edge is rounded to match the experimental airfoil. The trailing edge is modeled as a wedge which causes a slight increase in the chord length.

First, a steady-state prediction is run with the Euler code to ensure that the specified back pressure gives the desired inflow properties. An outflow static back pressure (p_2/p_{o_1}) of 0.6630 was found to give an average inlet Mach number (M_1) of 0.806. The steady pressure distributions are shown in Figure 7 for both the experimental data and the Euler code predictions. The agreement is good except near the leading edge on the lower surface. It should be noted that similar agreement is reported in reference 19 using a different Euler code reported in reference 7.

The same back pressure was then used in the unsteady predictions, which are shown in Figures 8 to 9 for the same respective interblade phase angles as the previous flat plate cascade with pitching motions about the midchord. The addition of loading to the cascade tends to change the unsteady loading over a good portion of the chordlength. The results from the Smith theory are repeated in these figures for relative comparisons even though they are valid only for flat plates. The experimental data are only included for σ = -90 degrees since the results for σ = 90 degrees are thought to be unreliable due to problems with the experimental cascade (ref.19). The Euler solutions and the experimental data show the same qualitative agreement, but differ quantitatively. The addition of loading causes a hump to occur in the pressures along the chord. Obviously, flat-plate theory cannot predict these effects and does not exhibit the same trends. Comparisons of the Euler solutions with the flat plate cases in Figures 3 and 4 demonstrate the difference in the unsteady pressure distributions due to loading. Additional cases were ran for M_1 = 0.55 and k = 0.20, but are not shown. These cases show the loading effects diminishing and the quantitative between the experiment, theory and the Euler solutions to be quite good for σ = -90, 0, and 90 degrees.

Linear/Nonlinear Behavior

One reason for developing a code capable of capturing nonlinear fluid behavior to solve oscillating cascade problems is to investigate and identify nonlinear/linear boundaries. There has been little work done to date to determine where linear theories cannot be applied to unsteady cascade flows. Dowell, et al. (ref.23) have studied nonlinear behavior in unsteady transonic flows for isolated airfoils. We will now extend this type of investigation to cascade flows. Two possible mechanisms for nonlinear behavior include strong shocks and separated flows. While the latter is beyond the scope of this paper, the present code can be used to investigate nonlinear behavior due to shock motions in oscillating cascades. The following results are a sample of such an investigation for limited cascade geometries and flow conditions.

Case 1

It is desirable to find a flow for a cascade with a strong normal shock located somewhere along the chordline of the airfoil. This has been done using the cascade of biconvex airfoils used in the previous section and lowering the back pressure (p_2/p_{o1} = 0.61) until a strong normal shock develops. The steady pressure distribution for this case is shown in Figure 10 and corresponds to: M_1 = 0.90, γ = 45 degrees, s/c = 1.538, and i = 2 degrees. The blades are now oscillated in torsion about their mid-chord for k = 0.32 and σ = 0 for various amplitudes of oscillation. If the flowfield is linear, the force coefficients would be a linear function of the pitching amplitude. Figure 11 shows a prediction for the first harmonic of the dynamic moment coefficient magnitude versus α_1. The smaller amplitudes (0.1 and 0.2) are expected to be linear and are the baseline for the "linear" solution shown in the figure. The predictions become nonlinear for amplitudes greater than about one degree. One can argue, however, that for all practical purposes, the solution can be treated as linear for even larger amplitudes. Figure 12 shows the normalized unsteady pressure difference distributions for the corresponding amplitudes of oscillation. To no surprise, the regions near the shocks are where the nonlinearity occur, whereas the regions away from the shocks are reasonably linear. Note that this behavior is very similar to the results reported by Dowell, et al. (ref.23) for isolated airfoils.

Case 2

For this case, the solidity is increased by about a factor of two from the above case. As the solidity is increased, it is harder to find a flow condition with a strong normal shock that does not choke the passage. Using p_2/p_{o1} = 0.690, M_1 = 0.72, γ = 45 degrees, s/c = 0.766, i = 2 degrees, k = 0.32; a mean flow with almost the maximum possible flow rate before choking the flow is obtained. Results from a study of the effects of pitching amplitudes are shown for σ = 0 degrees in Figure 13a and σ = 180 degrees in Figure 13b. For σ = 0 degrees, the trends are very similar to those found in the lower solidity cascade; pitching amplitudes greater than about one degree begin to deviate from linearity. However, when σ = 180 degrees, the deviation from linearity occurs for a pitching amplitude somewhere between 0.2 and 0.5 degrees. Inspection of the predicted flowfield reveals that the passages are choking over portions of the pitching cycle. This means that a small pitching amplitude can cause the cascade to choke intermittently when the mean flow is at the onset of choking. Several cases (not presented) were ran for various interblade phase angles at a slightly lower inlet Mach number and show the onset of non-linear behavior to be similar to case 1, for both σ = 0 and σ = 180 degrees.

Further parametric studies are needed for different blade geometries, pitching frequencies, motions, solidities, etc. to verify that the cases presented here are typical. For the flutter problem, the solutions of interest have small amplitudes and all of the solutions presented here for small oscillation amplitudes were found to be linear. A possible exception is when the response from the blade structure is included and a limit cycle behavior may require modeling higher amplitudes where the flow is nonlinear. In forced response problems, if the effective inflow angle to the blade changes by more than one degree, there may be nonlinearities in the unsteady flowfield when strong shocks are present, especially when the blade passages choke.

CONCLUSIONS

A code has been developed to solve the unsteady Euler equations for oscillating cascades. The code deforms the computational grid to model arbitrary motions for the airfoils. Predictions from the code for harmonically oscillating airfoils are compared to both theory and experimental data. The predictions for a cascade of flat plates with small pitching and plunging amplitudes are compared to small-perturbation theory and shows good overall agreement, except for certain cases operating in a super-resonant flowfield. Predictions are also compared to experimental data and show qualitative agreement. However, quantitative agreement is a function of the interblade phase angle and inflow Mach number.

An investigation of the nonlinear behavior in an oscillating cascade was done by varying the amplitude of pitching for a limited number of cases. Mean flows were selected with strong normal shocks on both the upper and lower surfaces of the airfoils. Based on the predicted unsteady moment coefficient, the responses become nonlinear for amplitudes greater than about one degree. The pressure distributions reveal that nonlinearities are most dominant near the shocks. Stronger nonlinearities occur when the blade passages choke over portions

of the pitching cycle. Intermittent choking can occur for small pitching amplitudes when the mean flow is at the onset of choking and is a function of the interblade phase angle. This code is a useful tool for identifying non-linear flowfield in oscillating cascades.

ACKNOWLEDGMENTS

The authors would like to thank Dr. Daniel Buffum, of NASA Lewis Research Center, for providing the experimental data and test cases for these comparisons; Mr. Timothy Beach, of Sverdrup Technology Inc., for providing the grid generator, Dr. Daniel Hoyniak, of NASA Lewis Research Center, for running the LINFLO solutions, and Dr. David Whitfield and Dr. Mark Janus, of Mississippi State University, for many helpful discussions concerning the flow algorithm.

REFERENCES

1. Nallasamy, M. and Groeneweg, J.F., "Prediction of Unsteady Blade Surface Pressures on an Advanced Propeller at an Angle of Attack," AIAA Paper 89-1060, November 1989.
2. Smith, S.N., "Discrete Frequency Sound Generation in Axial Flow Turbomachines," ARC-R/M-3709, 1971.
3. Verdon, J.M. and Casper, J.R., "A Linearized Unsteady Aerodynamic Analysis for Transonic Cascades," *Journal of Fluid Mechanics*, Vol. 149, December 1984, pp. 403-429.
4. Hall, K.C. and Crawley, E.F., "Calculation of Unsteady Flows in Turbomachinery Using the Linearized Euler Equations," Fourth Symposium on Unsteady Aerodynamics and Aeroelasticity of Turbomachines and Propellers, Aachen, West Germany, September 1987.
5. Kao, Y.F., "A Two-Dimensional Unsteady Analysis for Transonic and Supersonic Cascade Flows," Ph.D. Thesis, Purdue University, May 1989.
6. Fransson, T.H. and Pandolfi, M., "Numerical Investigation of Unsteady Subsonic Compressible Flows Through an Oscillating Cascade," ASME Paper 86-GT-304, June 1986.
7. Huff, D.L., "Numerical Analysis of Flow Through Oscillating Cascade Sections," AIAA Paper 89-0437, Jan. 1989.
8. He, L., "An Euler Solution for Unsteady Flows Around Oscillating Blades," ASME Paper 89-GT-279, June 1989.
9. Gerolymos, G.A., Blin, E., Quiniou, H., "Comparison of Inviscid Computations with Theory and Experiment in Vibrating Transonic Compressor Cascades," ASME Paper 90-GT-373, June 1990.
10. Bendiksen, O., "Aeroelastic Problems In Turbomachines," AIAA Paper 90-1157-CP, 1990.
11. Whitfield, D.L., Janus, J.M., and Simpson, L.B., "Implicit Finite Volume High Resolution Wave-Split Scheme for Solving the Unsteady Three-Dimensional Euler and Navier-Stokes Equations on Stationary or Dynamic Grids," Mississippi State Engineering and Industrial Research Station Report No. MSSU-EIRS-ASE-88-2, February, 1988.
12. Prewitt, Nathan C., "Two-Dimensional Euler Code for the Prediction of Pressure Distributions About an Airfoil," MS Thesis, Mississippi State University, Mississippi State, MS, December 1988.
13. Janus, J.M., "Advanced 3-D CFD Algorithm for Turbomachinery," PhD Dissertation, Mississippi State University, Mississippi State, MS, May 1989.
14. Arabshahi, A., "A Dynamic Multiblock Approach to Solving the Unsteady Euler Equations About Complex Configurations," PhD Dissertation, Mississippi State University, Mississippi State, MS, May 1989.
15. Whitfield, D.L., Janus, J.M., and Arabshahi, A., "Unsteady Euler Solutions on Dynamic Blocked Grids for Complex Configurations," AGARD Conference Proceedings, No.464, 1990.
16. Roe, P.L., "Approximate Rieman Solvers, Parameter Vectors, and Difference Schemes," *Journal of Computational Physics*, Vol. 43, pp. 357-372, 1981.
17. Beach, T.A., "An Interactive Grid Generation Procedure for Axial and Radial Flow Turbomachinery," AIAA Paper 90-0344, 1990.
18. Giles, M.B., "Calculation of Unsteady Wake/Rotor Interactions," AIAA Paper 87-0006, Jan. 1987.
19. Buffum, D.H. and Fleeter, S., "Aerodynamics Of A Linear Oscillating Cascade," NASA TM-103250, August 1990.

20. Janus, J.M., "The Development of A Three-Dimensional Split Flux Vector Solver with Dynamic Grid Applications," MS Thesis, Mississippi State University, Mississippi State, MS,August 1984.

21. Belk, D.M., "Three-Dimensional Euler Equations Solutions on Dynamic Blocked Grids," PhD Dissertation, Mississippi State University, Mississippi State, MS, August 1986.

22. Verdon, J.M. and Casper, J.R.; "Subsonic Flow Past an Oscillating Cascade with Finite Mean Flow Deflection," AIAA Journal, Vol. 18, No. 5, pp. 540-548, May 1980.

23. Dowell, E.H., Bland, S.R., and Williams, M.H., "Linear/Nonlinear Behavior in Unsteady Transonic Aerodynamics," AIAA Paper 81-0643, 1981.

Table 1. Unsteady moment coefficients about mid-chord, oscillating flat plate cascade, $M_1 = 0.80, k = 0.32, \gamma = 45°, s/c = 1.538, i = 0°, \alpha_1 = 1.2°$.

σ (deg)	C_m	Euler	Theory
−90	Re$\{C_m\}$	−.3466	−.3194
	Im$\{C_m\}$	−.8982	−.8567
0	Re$\{C_m\}$	−.4675	−.3724
	Im$\{C_m\}$	−.2931	−.3308
90 (α_1=1.2)	Re$\{C_m\}$	−.8553	−.5733
	Im$\{C_m\}$	−.5949	−.4301
90 (α_1=0.1)	Re$\{C_m\}$	−.8182	−.5733
	Im$\{C_m\}$	−.5456	−.4301

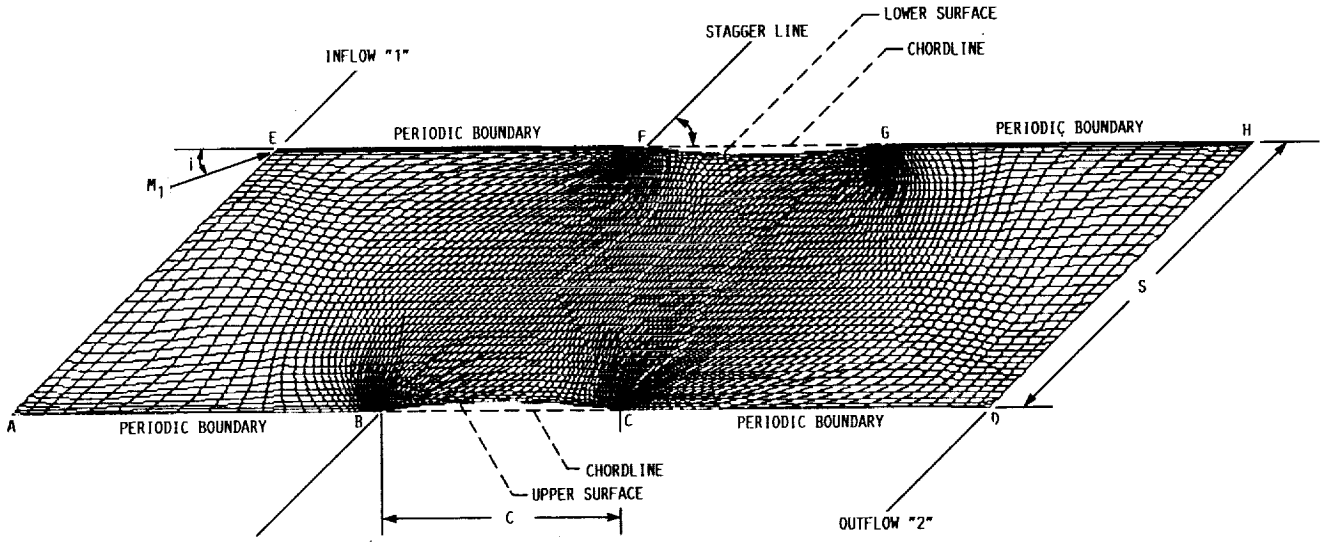

(a) One blade passage ($\sigma = 0°$).

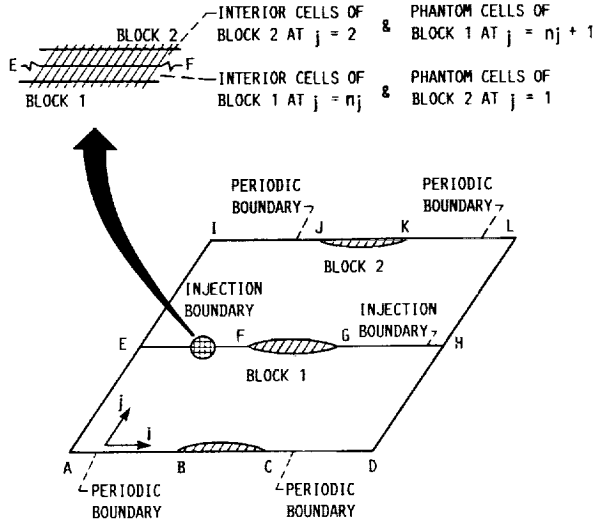

(b) Two blade passages ($\sigma = 180°$).

Figure 1. Grid and cascade geometry.

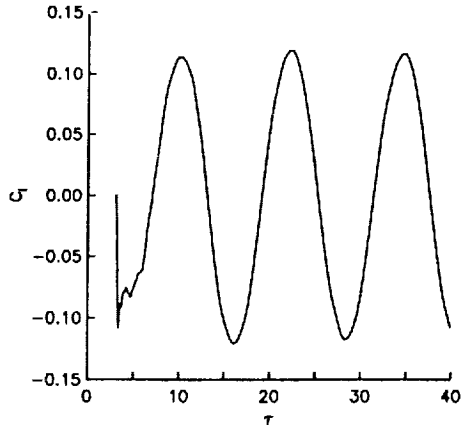

Figure 2. Lift coefficient vs. time, torsion oscillations of a flat plate cascade $M_1 = 0.80, k = 0.32, \gamma = 45°, s/c = 1.538, i = 0°, \alpha_1 = 1.2°, \sigma = -90°$.

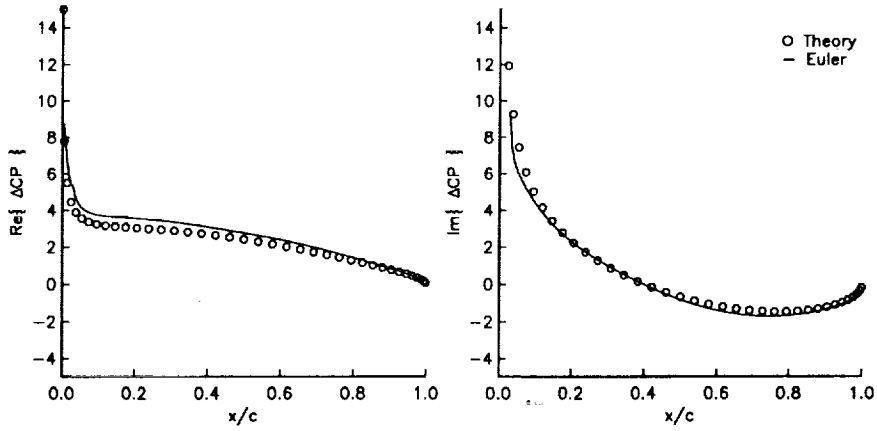

(a) Real (b) Imaginary

Figure 3. Unsteady pressure difference distribution, torsion oscillations of a flat plate cascade, $M_1 = 0.80, k = 0.32, \gamma = 45°, s/c = 1.538, i = 0°, \alpha_1 = 1.2°, \sigma = -90°$

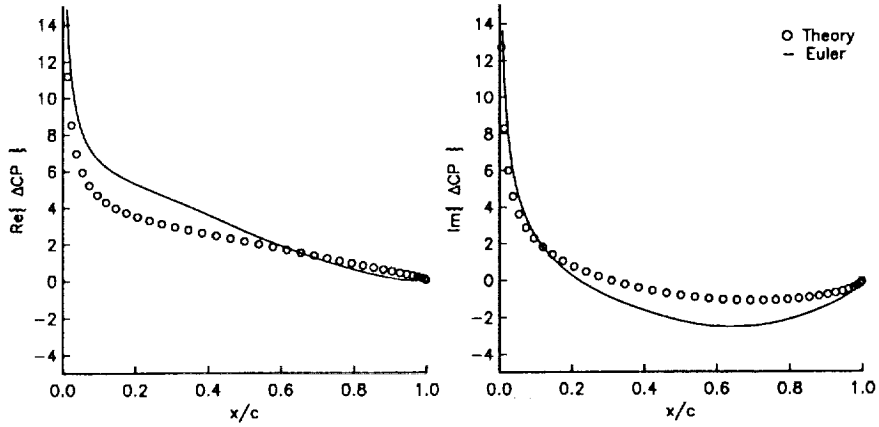

(a) Real (b) Imaginary

Figure 4. Unsteady pressure difference distribution, torsion oscillations of a flat plate cascade, $M_1 = 0.80, k = 0.32, \gamma = 45°, s/c = 1.538,$ $i = 0°, \alpha_1 = 1.2°, \sigma = 90°$

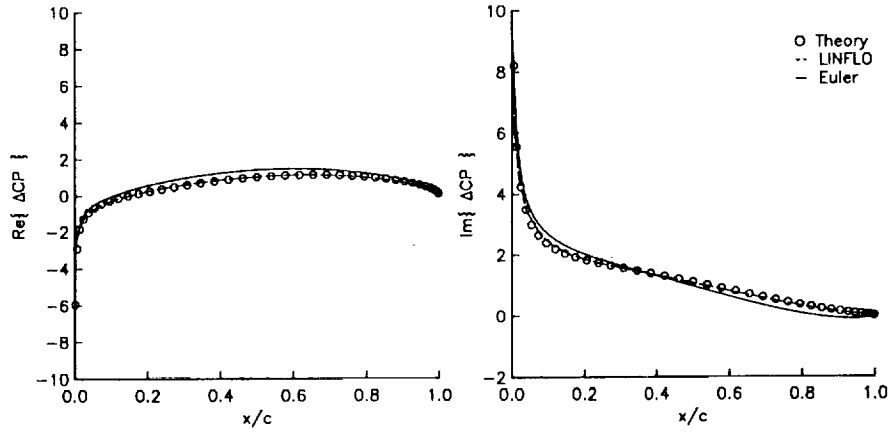

(a) Real (b) Imaginary

Figure 5. Unsteady pressure difference distribution, plunging oscillations of a flat plate cascade, $M_1 = 0.70, k = 0.50, \gamma = 45°, s/c = 1.0,$ $i = 0°, h_1 = 0.01$, $\sigma = 0°$.

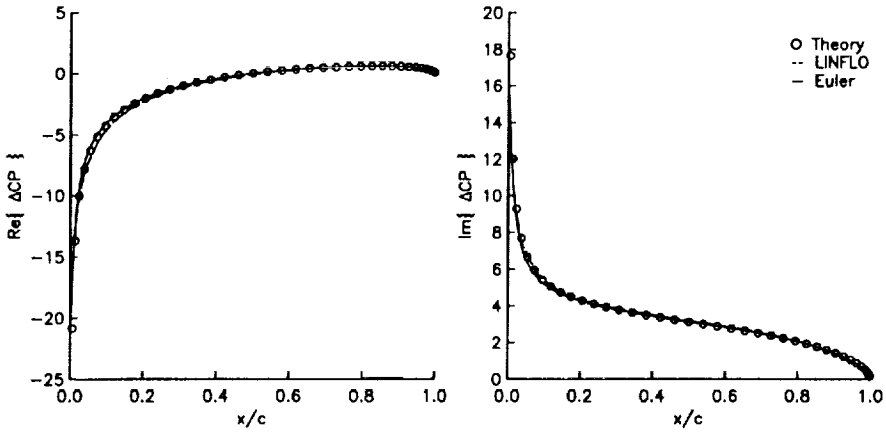

(a) Real (b) Imaginary

Figure 6. Unsteady pressure difference distribution, plunging oscillations of a flat plate cascade, $M_1 = 0.70, k = 0.50, \gamma = 45°, s/c = 1.0, i = 0°, h_1 = 0.01$, $\sigma = 180°$.

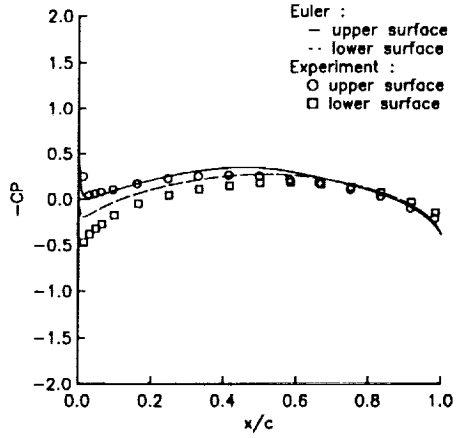

Figure 7. Steady pressure distribution, biconvex airfoil cascade, $M_1 = 0.80, \gamma = 45°, s/c = 1.538, i = 2°, \frac{p_2}{p_{01}} = 0.663$.

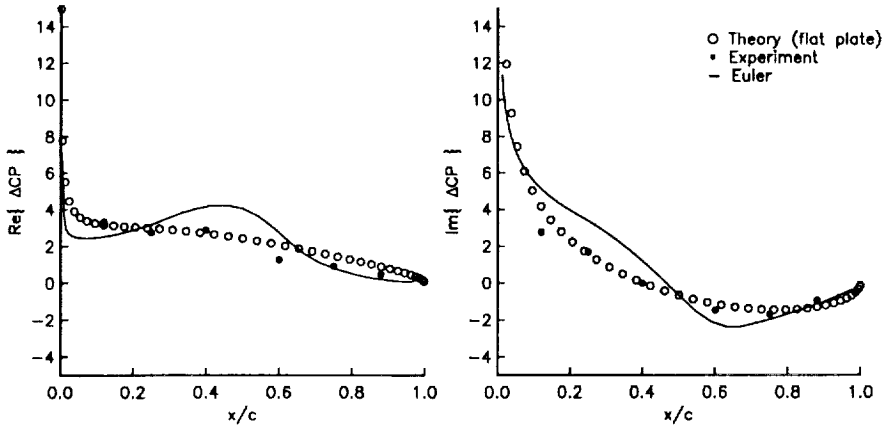

(a) Real (b) Imaginary

Figure 8. Unsteady pressure difference distribution, torsion oscillations of a biconvex airfoil cascade, $M_1 = 0.80, k = 0.32, \gamma = 45°, s/c = 1.538, i = 2°, \alpha_1 = 1.2°, \sigma = -90°$.

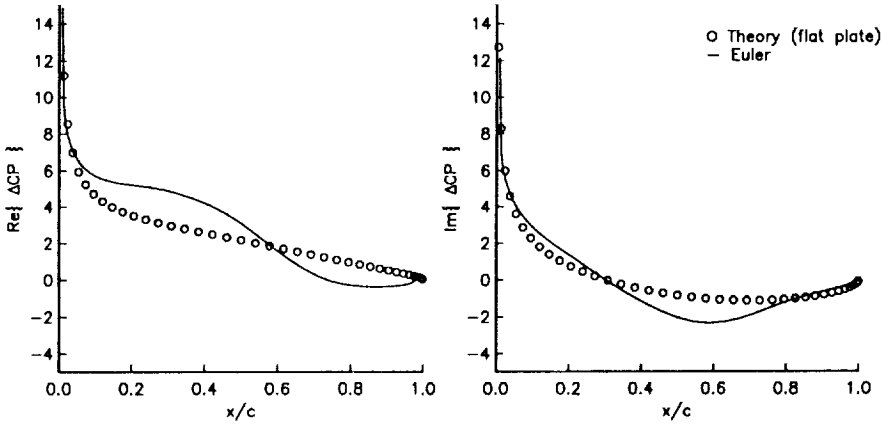

(a) Real (b) Imaginary

Figure 9. Unsteady pressure difference distribution, torsion oscillations of a biconvex airfoil cascade, $M_1 = 0.80, k = 0.32, \gamma = 45°, s/c = 1.538, i = 2°, \alpha_1 = 1.2°, \sigma = 90°$.

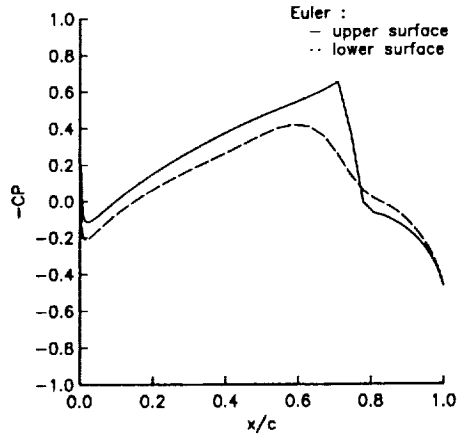

Figure 10. Steady pressure distribution, biconvex airfoil cascade, $M_1 = 0.90$, $\gamma = 45°$, $s/c = 1.538$, $i = 2°$, $\frac{p_2}{p_{01}} = 0.61$.

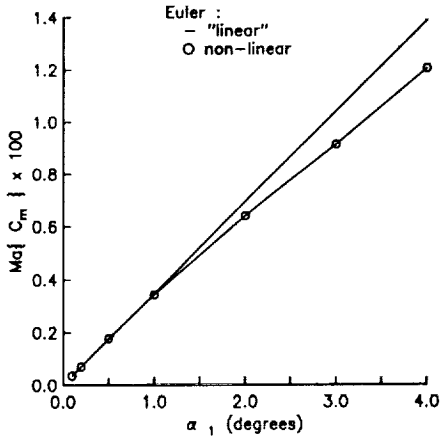

Figure 11. Unsteady moment coefficient about mid-chord vs. dynamic pitching amplitude, biconvex airfoil cascade, $M_1 = 0.90$, $k = 0.32$, $\gamma = 45°$, $s/c = 1.538$, $i = 2°$, $\frac{p_2}{p_{01}} = 0.61$, $\sigma = 0°$.

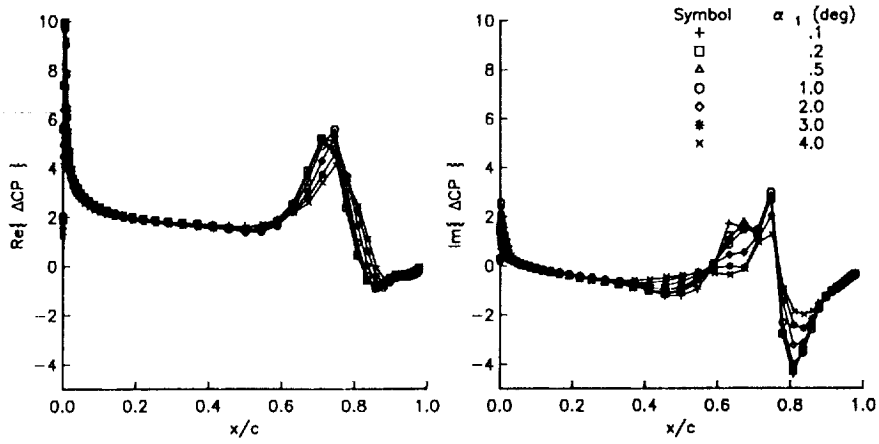

(a) Real (b) Imaginary

Figure 12. Unsteady pressure difference distribution, torsion oscillations of a biconvex airfoil cascade, $M_1 = 0.90, k = 0.32, \gamma = 45°, s/c = 1.538,$ $i = 2°, \frac{p_2}{p_{01}} = 0.61, \sigma = 0°.$

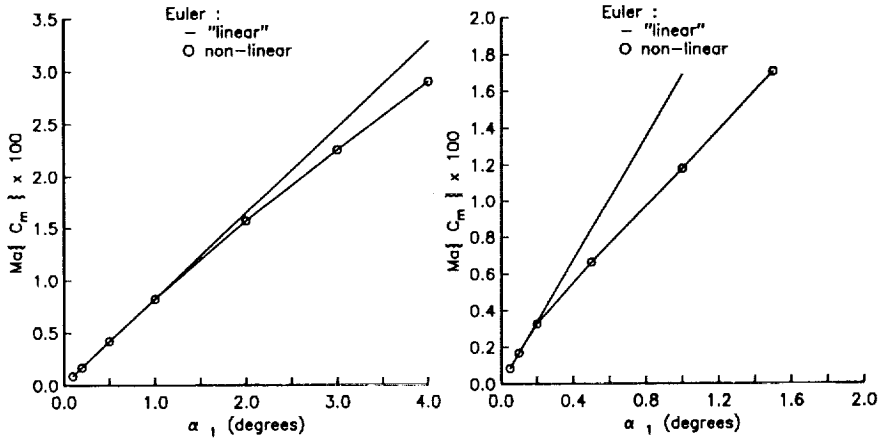

(a) $\sigma = 0°$ (b) $\sigma = 180°$

Figure 13. Unsteady moment coefficient about mid-chord vs. dynamic pitching amplitude, biconvex airfoil cascade, $M_1 = 0.72, k = 0.32, \gamma = 45°, s/c = 0.766,$ $i = 2°, \frac{p_2}{p_{01}} = 0.69.$

NASA
National Aeronautics and Space Administration

Report Documentation Page

1. Report No.	2. Government Accession No.	3. Recipient's Catalog No.
NASA TM -104377		

4. Title and Subtitle
Euler Flow Predictions for an Oscillating Cascade Using a High Resolution Wave-Split Scheme

5. Report Date

6. Performing Organization Code

7. Author(s)
Dennis L. Huff, Timothy W. Swafford, and T.S.R. Reddy

8. Performing Organization Report No.
E -5933

10. Work Unit No.
535-03-01

9. Performing Organization Name and Address
National Aeronautics and Space Administration
Lewis Research Center
Cleveland, Ohio 44135 - 3191

11. Contract or Grant No.

13. Type of Report and Period Covered
Technical Memorandum

12. Sponsoring Agency Name and Address
National Aeronautics and Space Administration
Washington, D.C. 20546 - 0001

14. Sponsoring Agency Code

15. Supplementary Notes
Prepared for the 36th International Gas Turbine and Aeroengine Congress and Exposition sponsored by the American Society of Mechanical Engineers, Orlando, Florida, June 3-6, 1991. Dennis L. Huff, NASA Lewis Research Center; Timothy W. Swafford, Mississippi State University, Mississippi State, Mississippi 39762 and Summer Faculty Fellow at NASA Lewis Research Center; T.S.R. Reddy, The University of Toledo, Toledo, Ohio 43606 and NASA Resident Research Associate. Responsible person, Dennis L. Huff, (216) 433-3913.

16. Abstract
A compressible flow code that can predict the nonlinear unsteady aerodynamics associated with transonic flows over oscillating cascades is developed and validated. The code solves the two-dimensional, unsteady Euler equations using a time-marching, flux-difference splitting scheme. The unsteady pressures and forces can be determined for arbitrary input motions, although this paper will only address harmonic pitching and plunging motions. The code solves the flow equations on a H-grid which is allowed to deform with the airfoil motion. Predictions are presented for both flat plate cascades and loaded airfoil cascades. Results are compared to flat plate theory and experimental data. Predictions are also presented for several oscillating cascades with strong normal shocks where the pitching amplitudes, cascade geometry and interblade phase angles are varied to investigate nonlinear behavior.

17. Key Words (Suggested by Author(s))	18. Distribution Statement
Unsteady aerodynamics; Flutter; Forced vibration; Airfoil oscillations; Nonlinearity	Unclassified - Unlimited Subject Category 02

19. Security Classif. (of the report)	20. Security Classif. (of this page)	21. No. of pages	22. Price*
Unclassified	Unclassified	18	A03

*For sale by the National Technical Information Service, Springfield, Virginia 22161